IEEE Access
Multidisciplinary ⋮ Rapid Review ⋮ Open Access Journal

Received 30 June 2023, accepted 23 July 2023, date of publication 26 July 2023, date of current version 4 August 2023.

Digital Object Identifier 10.1109/ACCESS.2023.3299168

RESEARCH ARTICLE

Full-Vectorial Bidirectional Beam Propagation Method for Nonradiative Dielectric Waveguides

HYUNUK AHN[1], (Student Member, IEEE), AKITO IGUCHI[1], (Member, IEEE), KEITA MORIMOTO[2], (Member, IEEE), AND YASUHIDE TSUJI[1], (Senior Member, IEEE)

[1]Division of Information and Electronic Engineering, Muroran Institute of Technology, Muroran, Hokkaido 050-0071, Japan
[2]Department of Electrical Engineering and Computer Science, University of Hyogo, Himeji, Hyogo 651-2197, Japan

Corresponding author: Akito Iguchi (iguchia@mmm.muroran-it.ac.jp)

This work was supported by the Japan Society for the Promotion of Science (JSPS) under Grant 20K22408, Grant 22K14296, and Grant 22K04234.

ABSTRACT We present a novel numerical analysis method called 1D full-vectorial finite element bidirectional beam propagation method (BiBPM) for the efficient design of nonradiative dielectric (NRD) waveguide components. The BiBPM is a field-based propagation operator method that does not require computing eigenpairs or diagonalizing characteristic matrixes. The dimension of the problem can be reduced in the case that the structure of the NRD guide does not vary in the perpendicular direction to its parallel perfect conductor plates. Moreover, since propagation operator methods eliminate the need to discretize in a homogeneous direction, a 3D problem can be converted into a 1D problem in specific situations. First, we analyze NRD guides with an offset and an air gap to verify the applicability of the transfer-matrix-based BiBPM to NRD guides. Given the instability of transfer matrix formulation, we also introduce the scattering-matrix-based BiBPM. Its validity is confirmed using numerical examples of an electromagnetic bandgap filter and a square resonator.

INDEX TERMS Bidirectional beam propagation method, finite element method, nonradiative dielectric waveguide, scattering matrix, transfer matrix.

I. INTRODUCTION

As a platform of millimeter-wave integrated circuits for 5G and beyond 5G systems, nonradiative dielectric (NRD) waveguides [1] are drawing attention. NRD guides are promising platforms for millimeter waves because of their nonradiation. The NRD guide shown in Fig. 1 consists of a dielectric waveguide sandwiched by parallel metal plates. Radiation into the air is prevented by keeping the distance of the metal plates shorter than half the wavelength in the air region, so this waveguide supports nonradiative longitudinal-section electric (LSE) and longitudinal-section magnetic (LSM) modes. Therefore, this NRD guide can aid in the miniaturization and integration of millimeter circuits. Numerical simulation is conducted many times to optimize the waveguide components of NRD integrated circuits. Thus, an efficient numerical simulation approach is required. For instance, band-stop or band-pass filters can be built using multiple resonators or stubs [2], [3], [4]. A high-dimensional optimization problem should be solved to obtain a broadband, flat-top filter response because multiple resonators or stubs may be necessary to achieve such a filter response. The use of efficient numerical methods is vital for high-dimensional optimization problems.

To solve waveguide discontinuity problems, mode-expansion-based techniques [5], [6], [7], the finite element method (FEM) [8], [9], and the finite-difference time-domain (FDTD) method [10] are well-established, widely used methods of solving waveguide discontinuity problems; these approaches are versatile but time consuming, especially for large-scale 3D full-vectorial problems. In previous works, to analyze discontinuity problems in NRD guides efficiently, two dimensional full vectorial (2DFV) approaches such as a 2DFV-FEM, have been introduced to analyze the discontinuity problems of NRD guides efficiently [11], [12], [13], [14]. Although 3D full-vectorial analysis is generally necessary

The associate editor coordinating the review of this manuscript and approving it for publication was Guido Lombardi.

to estimate propagation and scattering in NRD guides, the problem can be reduced to two dimensions in the case that the waveguide structure does not vary in the perpendicular direction to the parallel plates (z direction), thanks to the fields of LSE/LSM modes in the z direction can be represented by sinusoidal functions everywhere in the xy plane. For waveguide discontinuity problems, propagation operator methods can be used. These methods are advantageous, especially for waveguides composed of multiple homogeneous regions, because the problem dimension can be reduced, which eliminates the need to discretize in a homogeneous direction. The methods fall into two categories, namely, modal-based methods [15], [16], [17] and field-based methods, such as the bidirectional beam propagation method (BiBPM) [18], [19], [20], [21]. The BiBPM avoids computing eigenpairs or diagonalizing characteristic matrixes. Since 3D problems can be reduced to 1D problem, the BiBPM achieves efficient analysis by combining the idea of dimension-reduced approaches and propagation operator methods for specific situations.

In this paper, we propose the 1D full-vectorial finite element BiBPM for the discontinuity problems of NRD guides. In our method, the transverse direction is discretized using 1D edge-node line elements, where the z dependence of the field is expressed using a sinusoidal function. The procedure of a transfer-matrix-based BiBPM consists of computing a transfer operator $[T]$ that computes transmission and reflection at the waveguide discontinuity, and a propagator $[P]$ in a homogeneous layer. Transfer matrix formulation induces numerical instability [18] especially when the number of homogeneous layers is large, but scattering matrix formulation can avoid this instability. First, we introduce the transfer-matrix-based BiBPM to check the applicability of the BiBPM to the discontinuity problems of NRD guides. For the numerical validation of the transfer-matrix-based BiBPM, we show numerical examples of NRD guides with an offset and an air gap. We also develop the scattering-matrix-based BiBPM and validate it using numerical examples of an electromagnetic bandgap (EBG) filter and a square resonator. Since the results of 2DFV-FEM are equivalent to those of the well-established 3DFEM [11] if the waveguide structure is homogeneous in the z direction, we compare the results of the BiBPM with those of 2DFV-FEM for numerical verification.

II. FORMULATIONS

A. WAVE EQUATION IN HOMOGENEOUS LAYER

First, we assume that the NRD guide is homogeneous in the x direction and the electromagnetic wave propagates with a phase constant β_x as shown in Fig. 1. The functional of this system is

$$F(\mathbf{\Phi}) = \frac{1}{2}\iint_{\Omega}\left\{(\tilde{\nabla}\times\mathbf{\Phi}^*)\cdot([p]\tilde{\nabla}\times\mathbf{\Phi}) - k_0^2\mathbf{\Phi}^*\cdot[q]\mathbf{\Phi}\right\}dS + \frac{1}{2}\int_{\Gamma}\mathbf{\Phi}^*\cdot\{\mathbf{n}\times([p]\tilde{\nabla}\times\mathbf{\Phi})\}d\Gamma \quad (1)$$

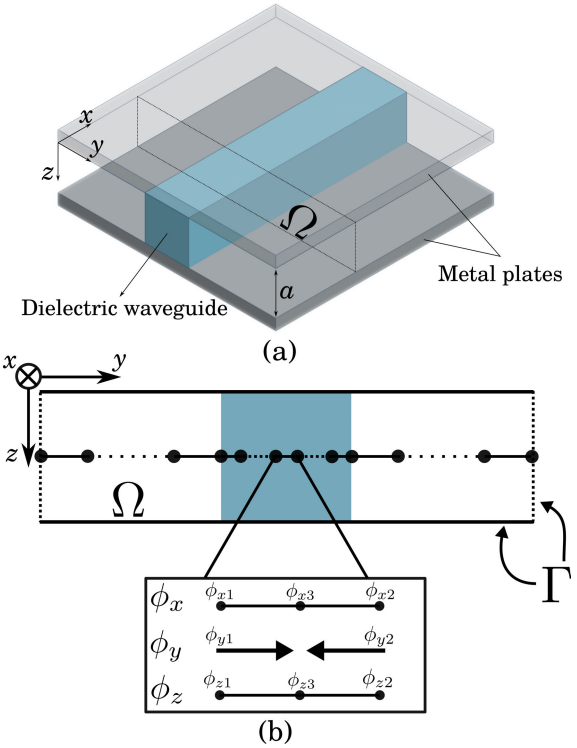

FIGURE 1. NRD guide that is homogeneous in x direction: (a) structure, (b) cross-sectional view.

where $\tilde{\nabla} = \{-j\beta_x,\ \partial/\partial y,\ \partial/\partial z\}^T$, and

$$[p] = \begin{cases} [\mu_r]^{-1} \\ [\varepsilon_r]^{-1} \end{cases}, \quad [q] = \begin{cases} [\varepsilon_r] \\ [\mu_r] \end{cases}, \quad \mathbf{\Phi} = \begin{cases} \sqrt{\varepsilon_0}\mathbf{E} \\ \sqrt{\mu_0}\mathbf{H} \end{cases}. \quad (2)$$

In (1), we assume that the top and bottom boundaries of the computational window are perfect electric conductors (PECs) and the left and right boundaries are Neumann boundaries, i.e. perfect magnetic conductors (PMCs) for $\mathbf{\Phi} = \sqrt{\varepsilon_0}\mathbf{E}$ or PECs for $\mathbf{\Phi} = \sqrt{\mu_0}\mathbf{H}$. $[\mu_r]$ and $[\varepsilon_r]$ are the relative permeability and permittivity tensors, respectively. Hereinafter, we consider the matrixes $[p]$ and $[q]$ to be diagonal matrixes.

$$[p] = \begin{bmatrix} p_x & 0 & 0 \\ 0 & p_y & 0 \\ 0 & 0 & p_z \end{bmatrix}, \quad [q] = \begin{bmatrix} q_x & 0 & 0 \\ 0 & q_y & 0 \\ 0 & 0 & q_z \end{bmatrix}.$$

We discretize Ω using edge-node hybrid line elements, as shown in Fig.1(b). We suppose that the electromagnetic field in an element is approximated by

$$\mathbf{\Phi}(x,y,z) = [N]^T\{\phi\}\exp(-j\beta_x x), \quad (3)$$

$$[N] = \begin{bmatrix} j\{N\}f(z) & \{0\} & \{0\} \\ \{0\} & \{V\}f(z) & \{0\} \\ \{0\} & \{0\} & \{N\}g(z) \end{bmatrix} \quad (4)$$

$$f(z) = \begin{cases} \sin(\kappa z) & (\mathbf{\Phi} = \sqrt{\varepsilon_0}\mathbf{E}) \\ \cos(\kappa z) & (\mathbf{\Phi} = \sqrt{\mu_0}\mathbf{H}) \end{cases}$$

$$g(z) = \begin{cases} \cos(\kappa z) & (\mathbf{\Phi} = \sqrt{\varepsilon_0}\mathbf{E}) \\ \sin(\kappa z) & (\mathbf{\Phi} = \sqrt{\mu_0}\mathbf{H}) \end{cases} \quad (5)$$

where $\{N\}$ and $\{V\}$ are shape function vectors for the nodal and edge elements, respectively; $\{\phi\} = \{\{\phi_x\}^T, \{\phi_y\}^T, \{\phi_z\}^T\}^T$, and $\kappa = \pi/a$. By substituting (3) into (1), and using the variational principle, we obtain the following generalized eigenvalue equation:

$$\left\{[A_{tt}] - \beta_x^2 \left([B_{tx}][A_{xx}]^{-1}[B_{xt}] - [C_{tt}]\right)\right\}\{\phi_t\} = \{0\}, \quad (6)$$

where $\{\phi_t\} = \{\{\phi_y\}^T, \{\phi_z\}^T\}^T$, and k_0 is a wave number in vacuum. $[A_{xx}]$, $[A_{tt}]$, $[B_{tx}]$ and $[C_{tt}]$ are defined as

$$[A_{tt}] = \begin{bmatrix}[A_{yy}] & [A_{yz}] \\ [A_{zy}] & [A_{zz}]\end{bmatrix} \quad (7)$$

$$[B_{tx}] = \begin{bmatrix}[B_{yx}] \\ [B_{zx}]\end{bmatrix} = [B_{xt}]^T \quad (8)$$

$$[C_{tt}] = \begin{bmatrix}[C_{yy}] & [0] \\ [0] & [C_{zz}]\end{bmatrix} \quad (9)$$

$$[A_{xx}] = \sum_{i=1}^{N_e} \int_{e_i} \left(p_y \kappa^2 \{N\}\{N\}^T + p_z \frac{\partial\{N\}}{\partial y}\frac{\partial\{N\}^T}{\partial y} - k_0^2 q_x \{N\}\{N\}^T\right) dy \quad (10)$$

$$[A_{yy}] = \sum_{i=1}^{N_e} \int_{e_i} \left(p_x \kappa^2 \{V\}\{V\}^T - k_0^2 q_y \{V\}\{V\}^T\right) dy \quad (11)$$

$$[A_{yz}] = \sum_{i=1}^{N_e} \int_{e_i} \left(-p_x u\kappa \{V\}\frac{\partial\{N\}^T}{\partial y}\right) dy = [A_{zy}]^T \quad (12)$$

$$[A_{zz}] = \sum_{i=1}^{N_e} \int_{e_i} \left(p_x \frac{\partial\{N\}}{\partial y}\frac{\partial\{N\}^T}{\partial y} - k_0^2 q_z \{N\}\{N\}^T\right) dy \quad (13)$$

$$[B_{xy}] = \sum_{i=1}^{N_e} \int_{e_i} p_z \frac{\partial\{N\}}{\partial y}\{V\}^T dy = [B_{yx}]^T \quad (14)$$

$$[B_{xz}] = \sum_{i=1}^{N_e} \int_{e_i} p_y u\kappa \{N\}\{N\}^T dy = [B_{zx}]^T \quad (15)$$

$$[C_{yy}] = \sum_{i=1}^{N_e} \int_{e_i} p_z \{V\}\{V\}^T dy \quad (16)$$

$$[C_{zz}] = \sum_{i=1}^{N_e} \int_{e_i} p_y \{N\}\{N\}^T dy \quad (17)$$

where

$$u = \begin{cases} 1 & (\mathbf{\Phi} = \sqrt{\varepsilon_0}\mathbf{E}) \\ -1 & (\mathbf{\Phi} = \sqrt{\mu_0}\mathbf{H}) \end{cases} \quad (18)$$

and N_e is the number of elements.

Next, we consider an NRD guide that has discontinuity in the x direction as shown in Fig. 2. By replacing β_x in (6) with $j\partial/\partial x$, we obtain the following wave equation in a layer that is homogeneous in the x direction:

$$\frac{\partial^2\{\phi_t\}}{\partial x^2} + [Q]\{\phi_t\} = \{0\} \quad (19)$$

where $[Q]$ is defined by

$$[Q] = \left([B_{tx}][A_{xx}]^{-1}[B_{xt}] - [C_{tt}]\right)^{-1}[A_{tt}]. \quad (20)$$

The solution of (19) in the kth layer is

$$\{\phi_t(x)\} = \exp(-j\sqrt{[Q]_k}(x - x_{k-1}))\{\phi_t(x_{k-1}^+)\}^{\mathrm{F}} + \exp(j\sqrt{[Q]_k}(x - x_k))\{\phi_t(x_k^-)\}^{\mathrm{B}} \quad (21)$$

where $x_k^{+/-}$ indicate the right/left limit at the point of discontinuity between the kth and $(k+1)$th layers. The first term on the right-hand side of the expression means a forward-propagating wave, and the second term means a backward-propagating wave. The method of computing $\sqrt{[Q]_k}$ is an important issue in the BiBPM. We compute $\sqrt{[Q]_k}$ using Schur decomposition [22] with branch-cut.

$$[Q]_k \exp(-j\alpha) = [\widehat{Q}]_k = [R]_k[\widehat{U}]_k[R]_k^\dagger \quad (22)$$

$$\sqrt{[Q]_k} = [R]_k\sqrt{[\widehat{U}]_k}\exp\left(j\frac{\alpha}{2}\right)[R]_k^\dagger \quad (23)$$

$$[\widehat{U}]_k = \begin{bmatrix} \widehat{u}_{k,11} & \widehat{u}_{k,12} & \widehat{u}_{k,13} & \cdots & \widehat{u}_{k,1n} \\ 0 & \widehat{u}_{k,22} & \widehat{u}_{k,23} & \cdots & \widehat{u}_{k,2n} \\ \vdots & \vdots & \vdots & \ddots & \vdots \\ 0 & 0 & 0 & \cdots & \widehat{u}_{k,nn} \end{bmatrix} \quad (24)$$

$$\sqrt{[\widehat{U}]}_k = \begin{bmatrix} \sqrt{\widehat{u}_{k,11}} & \widehat{v}_{k,12} & \widehat{v}_{k,13} & \cdots & \widehat{v}_{k,1n} \\ 0 & \sqrt{\widehat{u}_{k,22}} & \widehat{v}_{k,23} & \cdots & \widehat{v}_{k,2n} \\ \vdots & \vdots & \vdots & \ddots & \vdots \\ 0 & 0 & 0 & \cdots & \sqrt{\widehat{u}_{k,nn}} \end{bmatrix} \quad (25)$$

where $[R]_k$ is a unitary matrix obtained by the Schur decomposition, $[\widehat{U}]_k$ indicates the Schur form, α is the rotation angle of the branch cut and set to $\alpha = -\pi/4$ in this paper. The propagator in a layer is computed by reusing $[R]_k$ and $[U]_k$ as follows:

$$[P]_k^{\mathrm{F}} = \exp(-j\sqrt{[Q]_k}\Delta x_k) = [R]_k \exp(-j\sqrt{[U]_k}\Delta x_k)[R]_k^\dagger \quad (26)$$

Then, we factorize the exponential term as follows:

$$\begin{aligned}&\exp(-j\sqrt{[U]_k}\Delta x_k) \\ &\quad = \exp(j\beta_{0k}\Delta x_k)\exp(-j(\sqrt{[U]_k} + \beta_{0k}[I])\Delta x_k) \\ &\quad = \exp(j\beta_{0k}\Delta x_k)\exp(-j[G]_k\Delta x_k)\end{aligned} \quad (27)$$

where Δx_k is the layer thickness and β_{0k} is the reference phase constant. As the diagonal elements of $\sqrt{[U]}$ are phase constants, we choose β_{0k} as the average value of the propagating modes. We apply Padé (p, q) approximation [23] to $\exp(-j[G]_k\Delta x_k)$:

$$\begin{aligned}\exp(-j[G]_k\Delta x_k) &= [D]_k^{-1}[N]_k \\ [N]_k &= \sum_{i=0}^{p} a_i(-j[G]_k\Delta x_k)^i, \quad [D]_k \\ &= \sum_{i=0}^{q} b_i(j[G]_k\Delta x_k)^i\end{aligned} \quad (28)$$

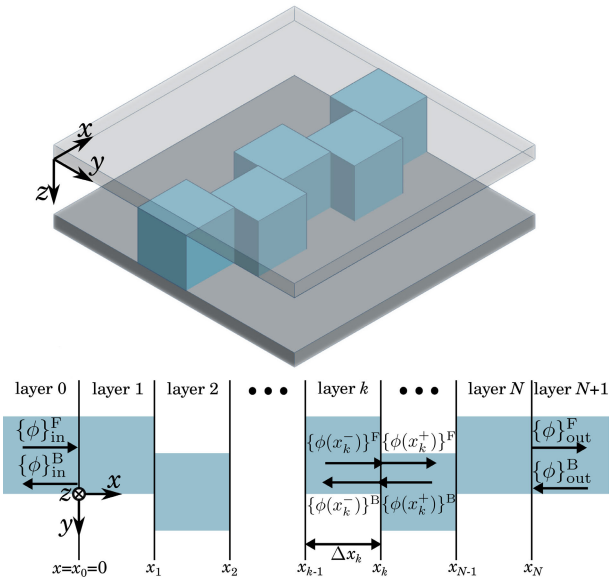

FIGURE 2. NRD guide with waveguide discontinuity.

where a_i and b_i are

$$a_i = \frac{(p+q-i)!p!}{(p+q)!i!(p-i)!} \tag{29}$$

$$b_i = \frac{(p+q-i)!q!}{(p+q)!i!(q-i)!}. \tag{30}$$

B. TRANSFER MATRIX FORMULATION

In this subsection, we introduce the transfer-matrix-based BiBPM. Through the continuity of $\{\phi_t\}$ and the power flow at the waveguide discontinuity, the following equations are obtained:

$$\left\{\phi_t\left(x_k^-\right)\right\}^{\mathrm{F}} + \left\{\phi_t\left(x_k^-\right)\right\}^{\mathrm{B}} = \left\{\phi_t\left(x_k^+\right)\right\}^{\mathrm{F}} + \left\{\phi_t\left(x_k^+\right)\right\}^{\mathrm{B}} \tag{31}$$

$$[F]_k\left\{\phi_t(x_k^-)\right\}^{\mathrm{F}} - [F]_k\left\{\phi_t(x_k^-)\right\}^{\mathrm{B}} = [F]_{k+1}\left\{\phi_t(x_k^+)\right\}^{\mathrm{F}} - [F]_{k+1}\left\{\phi_t(x_k^+)\right\}^{\mathrm{B}} \tag{32}$$

where $[F]_k$ is a matrix related to power and defined as

$$P_k = \frac{c}{4k_0}\{\phi_t\}^{\dagger}[F]_k\{\phi_t\} \tag{33}$$

$$[F]_k \equiv \left([C_{tt}]_k - [B_{tx}]_k[A_{xx}]_k^{-1}[B_{xt}]_k\right)\sqrt{[Q]_k} \tag{34}$$

where c is the speed of light in vacuum. From (26), (31), and (32), assuming that $\{\phi\}^{\mathrm{B}}_{\mathrm{out}} = \{0\}$, we obtain the following relation:

$$\begin{Bmatrix}\{\phi_t(x_N^+)\}^{\mathrm{F}}\\ \{0\}\end{Bmatrix} = [M]\begin{Bmatrix}\{\phi_t(x_0^-)\}^{\mathrm{F}}\\ \{\phi_t(x_0^-)\}^{\mathrm{B}}\end{Bmatrix} \tag{35}$$

$$[M] = [T]_N[P]_N[T]_{N-1}[P]_{N-1}\cdots[T]_1[P]_1[T]_0 \tag{36}$$

where $\{\phi_t(x_0^-)\}^{\mathrm{F}}$ indicates the input field. $\{\phi_t(x_N^+)\}^{\mathrm{F}}$ and $\{\phi_t(x_0^-)\}^{\mathrm{B}}$ are the transmission and reflection fields, respectively. In (36), the propagation operator in the homogeneous

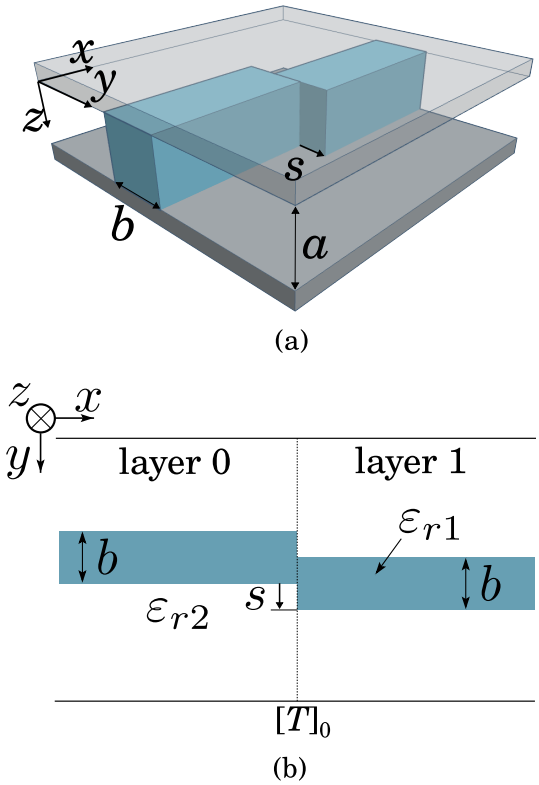

FIGURE 3. NRD guide with an offset: (a) bird's-eye view, (b) top view.

layer $[P]_k$ is

$$\begin{bmatrix}\{\phi_t(x_k^-)\}^{\mathrm{F}}\\ \{\phi_t(x_k^-)\}^{\mathrm{B}}\end{bmatrix} \equiv \begin{bmatrix}[P]_k^{\mathrm{F}} & [0]\\ [0] & ([P]_k^{\mathrm{F}})^{-1}\end{bmatrix}\begin{bmatrix}\{\phi_t(x_{k-1}^+)\}^{\mathrm{F}}\\ \{\phi_t(x_{k-1}^+)\}^{\mathrm{B}}\end{bmatrix} \tag{37}$$

and the operator at the discontinuity boundary $[T]_k$ is

$$[T]_k \equiv \frac{1}{2}\begin{bmatrix}[I]+[F]_{k+1}^{-1}[F]_k & [I]-[F]_{k+1}^{-1}[F]_k\\ [I]-[F]_{k+1}^{-1}[F]_k & [I]+[F]_{k+1}^{-1}[F]_k\end{bmatrix}. \tag{38}$$

However, this formulation is unstable, especially when a device consists of a large number of layers, because evanescent modes with extremely large $\mathrm{Im}\{\beta_x\}$ grow dramatically due to $([P]_k^F)^{-1}$. A scattering-matrix-based formulation enables stable computation, so we introduce the scattering-matrix-based BiBPM in the next subsection.

C. SCATTERING MATRIX FORMULATION

A scattering matrix is defined as

$$\begin{bmatrix}\{\phi_t(x_0^-)\}^{\mathrm{B}}\\ \{\phi_t(x_N^+)\}^{\mathrm{F}}\end{bmatrix} = \begin{bmatrix}[S_{11}(x_0^-)] & [S_{12}(x_N^+)]\\ [S_{21}(x_0^-)] & [S_{22}(x_N^+)]\end{bmatrix}\begin{bmatrix}\{\phi_t(x_0^-)\}^{\mathrm{F}}\\ \{\phi_t(x_N^+)\}^{\mathrm{B}}\end{bmatrix} \tag{39}$$

where $[S_{11/21}(x')]$ indicates the $S_{11/21}$ in $x' < x < x_N^+$ and $[S_{12/22}(x')]$ indicates the $S_{12/22}$ in $x_0^- < x < x'$. From the definition of the scattering matrix, we obtain

$$[S_{11}(x_N^+)] = [0] \tag{40}$$

$$[S_{21}(x_N^+)] = [I]. \tag{41}$$

Using the continuity condition of $\{\phi_t\}$ and the power at the waveguide discontinuity, we obtain the following relation:

$$[S_{11}(x_N^-)] = ([I]+[C]_N)^{-1}([I]-[C]_N) \tag{42}$$

$$[S_{21}(x_N^-)] = [S_{21}(x_N^+)]([I] + [S_{11}(x_N^+)])^{-1}([I] + [S_{11}(x_N^-)]) \tag{43}$$

where $[C]_k$ is

$$[C]_k \equiv [F]_k^{-1}[F]_{k+1}([I] - [S_{11}(x_k^+)])([I] + [S_{11}(x_k^+)])^{-1}. \tag{44}$$

Using the definition of $[P]_k^{\mathrm{F}}$, we obtain the following relation:

$$[S_{11}(x_{N-1}^+)] = [P]_N^{\mathrm{F}}[S_{11}(x_N^-)][P]_N^{\mathrm{F}} \tag{45}$$

$$[S_{21}(x_{N-1}^+)] = [S_{21}(x_N^-)][P]_N^{\mathrm{F}}. \tag{46}$$

By iterating the process described in (42)−(46) from $k = N$ to 0, we obtain the scattering matrix of the whole system. $[S_{12}(x_N^+)]$ and $[S_{22}(x_N^+)]$ are obtained via the same way. We call this process BiBPM-S, where only $[S_{11/21}(x')]$ is computed. If the waveguide has the large number of periods, then the use of the Redheffer star product can make the BiBPM efficient. The scattering matrix of the whole system is computed as

$$[S] = [S]_{\mathrm{out}} \star [S]_\Lambda \star \cdots \star [S]_\Lambda \star [S]_{\mathrm{in}} \tag{47}$$

where $\star$ is the Redheffer star product [24], $[S]_{\mathrm{in/out}}$ is the scattering matrix of the input/output system, and $[S]_\Lambda$ is the scattering matrix of one period system. Moreover, the computation of the star product can be reduced. For example, to calculate 20 times the star product $[S]_{20,\Lambda}$, we compute $[S]_{2^n,\Lambda}(n = 1, 2, 3, 4)$ and then obtain $[S]_{20,\Lambda} = [S]_{2^4,\Lambda} \star [S]_{2^2,\Lambda}$. In this case, we multiply five times, not 20 times. This process of using the Redheffer star product is hereinafter called BiBPM-R.

III. NUMERICAL EXAMPLE

A. TRANSFER MATRIX BASED BiBPM

First, the analysis results for the NRD guide with an offset are shown to demonstrate the validity of the transfer-matrix-based BiBPM. In this example, we verify the operator at the waveguide discontinuity $[T]$. The structural parameters shown in Fig. 3 are as follows: the distance between metal plates is $a = 2.25$ mm; the width of the dielectric waveguide is $b = 2$ mm; the relative permittivities of the dielectric waveguide and air are $\varepsilon_{r1} = 2.2$ and $\varepsilon_{r2} = 1$, respectively; and s is the waveguide offset. An LSM_{01} wave at a frequency of 60 GHz is launched to the surface between layers 0 and 1. Here we investigate the dependence of the transmission power on the offset s. Figure 4 shows the transmission power of the LS modes as a function of the offset. Findings indicate that as the offset s increases, the transmission power of LSM_{01} decreases and slightly changes to LSE_{01} mode. For comparison, 2DFV-FEM results are also shown in Fig. 4. The two sets of results agree well, which indicates the validity of $[T]$.

Next, we analyze a NRD guide with an air gap to show the validity of one homogeneous layer's matrix $[P]$, which is also used in the scattering-matrix-based BiBPM. The structural parameters shown in Fig. 5, frequency, and input mode in this

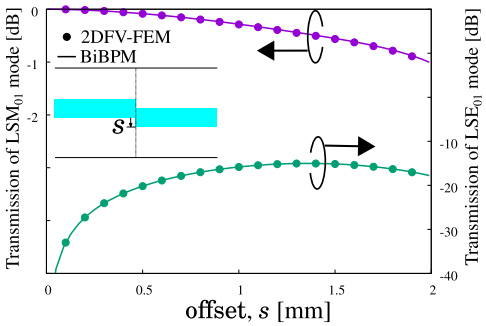

FIGURE 4. Transmission of LSM_{01} and LSE_{01} modes as a function of offset. The LSM_{01} wave at 60 GHz is launched from layer 0. The solid line indicates the BiBPM results, and the dots denote the 2DFV-FEM results.

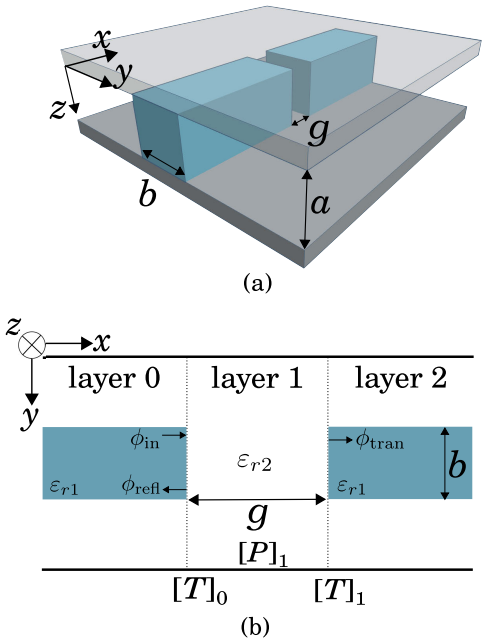

FIGURE 5. NRD guide with an airgap: (a) bird's-eye view, (b) top view.

analysis are the same as those in the previous example except the air gap g. In this example, we investigate the dependence of the transmission and reflection power of the LSM_{01} mode on air gap g.

Figure 6 shows the transmission and reflection power of the LSM_{01} mode as a function of the air gap g. The effect of the order of Padé approximation is also shown in this figure. In Fig. 6(a), although the difference between the BiBPM and 2DFV-FEM is slight in the small-gap region, the BiBPM results slightly deviate from the 2DFV-FEM results in the large-gap region, as shown in the inset. This is because not all the evanescent modes in the air gap can be estimated through Padé approximation. Nevertheless, we achieve high accuracy using high-order Padé approximation.

B. SCATTERING MATRIX BASED BiBPM

In this section, we analyze an EBG filter and a square resonator to demonstrate the validity of the scattering-matrix-based BiBPM.

The structural parameters shown in Fig. 7 except b', r, Λ and the input mode are the same as in the previous example.

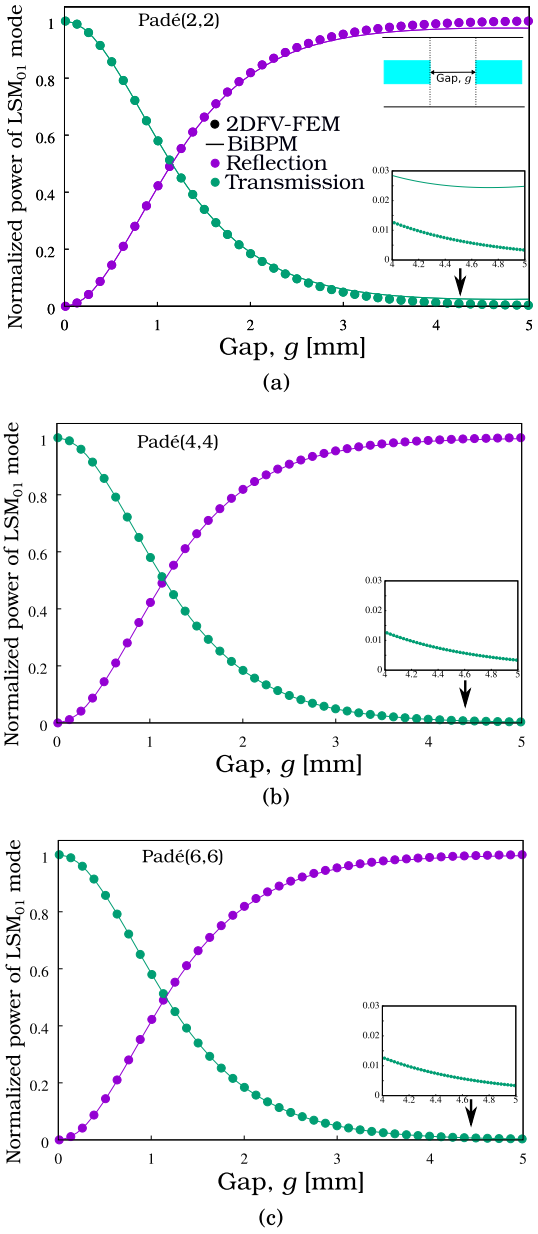

FIGURE 6. Normalized power of LSM_{01} mode as function of air gap. The LSM_{01} wave at 60 GHz is launched from layer 0. The solid line indicates the BiBPM results, and the dots denote the 2DFV-FEM results. The orders of Padé approximation are (a) (2,2), (b) (4,4), and (c) (6,6).

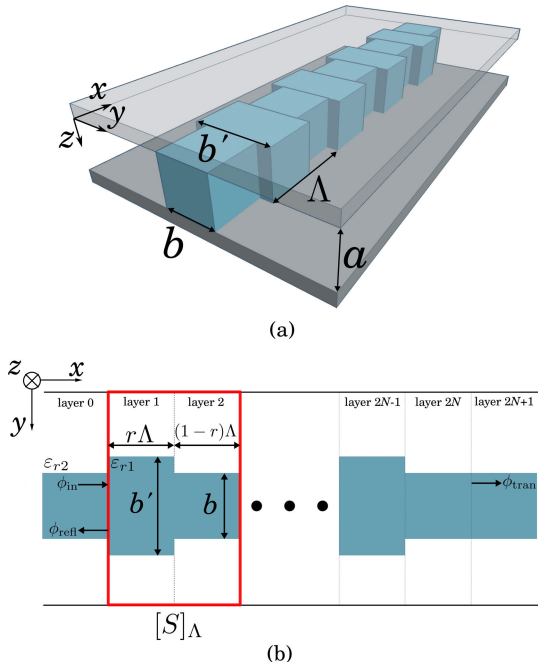

FIGURE 7. NRD guide with EBG filter: (a) bird's-eye view, (b) top view.

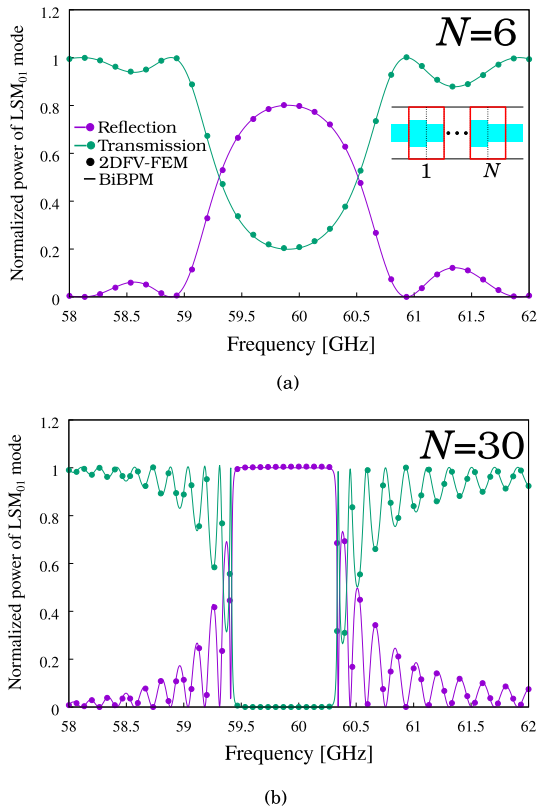

FIGURE 8. Transmission and reflection power spectra of LSM_{01} mode in EBG filter. The EBG period numbers are (a) N=6 and (b) N=30.

Here, the duty ratio is $r = 0.5$, the thick core width is $b' = 3$ mm, and we set $\Lambda = 8.12$ mm so that the center of the stop band is 60 GHz. In this example, we investigate the frequency characteristics of the transmission power, reflection power, and computational time between the scattering-matrix-based BiBPM and 2DFV-FEM.

The frequency characteristics of the EBG filter are shown in Fig. 8. The stop band is in the vicinity of 60 GHz. The results of the scattering-matrix-based BiBPM agree well with those of 2DFV-FEM, which indicates the validity of the proposed method. The dependence of the period number N on computational time is shown in Fig. 9. In this comparison, we use a computer with an Intel Core i7-13700KF (3.4 GHz) processor. The BiBPM is faster than 2DFV-FEM when the period number is more than 1 or 2. Moreover, as the period number increases, BiBPM-R becomes more efficient than BiBPM-S, as expected.

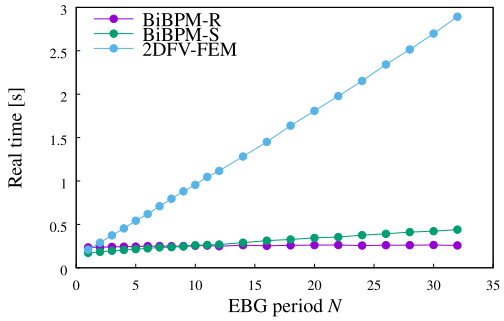

FIGURE 9. Dependence of computational time on EBG period.

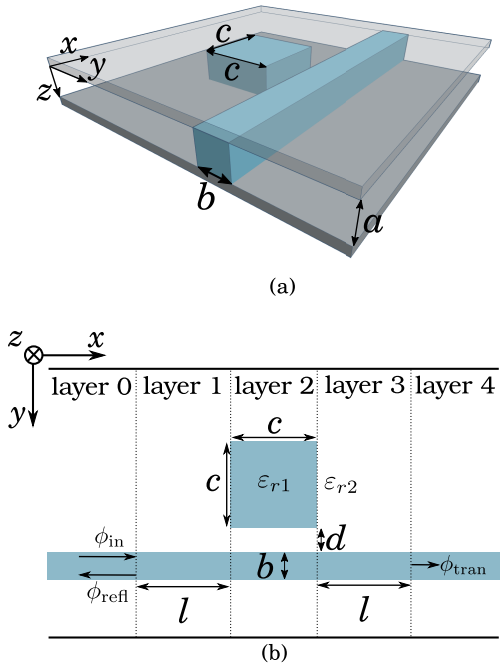

FIGURE 10. The bird's eye view of square resonator, and (b) its top view.

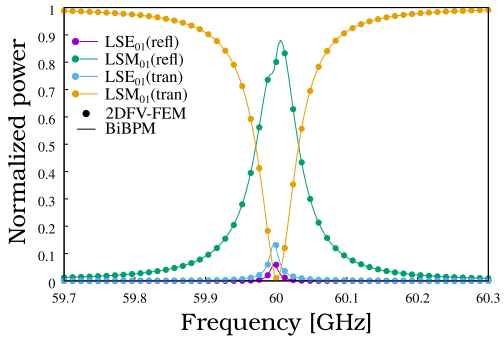

FIGURE 11. Normalized power spectra of LS modes in square resonator.

Finally, we analyze a square resonator. The structure of the resonator is shown in Fig. 10. The structural parameters shown in Fig. 10 are the same as in the previous example except $c = 5.88$ mm, $l = 10$ mm, and $d = 2.5$ mm, and the input mode. The resonator size c is determined so that the resonance frequency is approximately 60 GHz.

The transmission and reflection power spectra of the LS modes are shown in Fig. 11. Because of the asymmetric structure, a slight mode transformation to the LSE_{01} mode occurs around the resonance frequency. Moreover, in this example, both results agree well, which indicates that the BiBPM can consider various modes propagating in the square resonator at various angles.

TABLE 1. Comparison of the 3DFEM, the 2DFV-FEM, and the 1DFV-BiBPM.

	Waveguide variation[a] in z-direction	Waveguide variation[a] in xy-direction	Cost
3DFEM	Arbitrary	Arbitrary	High
2DFV-FEM [11]	Uniform	Arbitrary	Low
1DFV-BiBPM	Uniform	Staircase	Very low[b]

[a] "Arbitrary" means the methods can model arbitrary waveguide profile in the direction. "Uniform" or "Staircase" indicates applicable waveguide profiles are limited to uniform or staircase. z is a perpendicular direction to the parallel plates.
[b] If a waveguide has periodic structures or longitudinally uniform sections, the computational cost is very low.

IV. CONCLUSION

We develop the novel 1D full-vectorial BiBPM for NRD guides. First, we introduce the transfer-matrix-based BiBPM and examine its validity using analysis results for NRD guides with an offset and an air gap. The findings for the air gap show that accuracy can be controlled using the order of Padé approximation. Next, we develop the scattering-matrix-based BiBPM, which resolves the numerical instability of transfer matrix formulation, and validate it using analysis results for an EBG filter and a square resonator. According to the EBG filter results, the BiBPM can be more efficient than 2DFV-FEM when the number of periods is large. The results for the resonator suggests that the BiBPM can consider various modes propagating in the square resonator at various angles.

We summarized the characteristics of the 3DFEM, the 2DFV-FEM [11], and the 1DFV-BiBPM in Table 1. The proposed method and the 2DFV-FEM have a limitation that the waveguide should be uniform in perpendicular direction to the parallel plates. In addition, the waveguide profile should be a staircase or is interpreted as a staircase profile in the 1DFV-BiBPM. Although the propagator $[P]$ is approximated in the 1DFV-BiBPM, as shown in Section III-A the accuracy can be controlled by using the high-order Padé approximation. The proposed BiBPM is based on a strategy of reducing the problem dimension using the characteristics of the waves propagating in the NRD guide and a propagation operator method. The BiBPM offers advantages for the optimal design of NRD guide components that have long, uniform structures in the transmission axis or are constructed using multiple resonators or stubs.

REFERENCES

[1] T. Yoneyama and S. Nishida, "Nonradiative dielectric waveguide for millimeter-wave integrated circuits," *IEEE Trans. Microw. Theory Techn.*, vol. MTT-29, no. 11, pp. 1188–1192, Nov. 1981.

[2] T. Yoneyama, F. Kuroki, and S. Nishida, "Design of nonradiative dielectric waveguide filters (short papers)," *IEEE Trans. Microw. Theory Techn.*, vol. MTT-32, no. 12, pp. 1659–1662, Dec. 1984.

[3] J. Huang and K. Wu, "A two-path multimode bandpass filters using the nonradiative dielectric (NRD) waveguide technology," *IEEE MTT-S Int. Microw. Symp. Dig.*, May 1995, vol. 29, no. 11, pp. 1188–1192.
[4] H. Hanen, L. Lassaad, G. Ali, and G. Abdelehafidh, "Design of pass band filter based on NRD-guide with the iterative method," in *Proc. Int. Conf. Adv. Comput. Appl. (ICCAT)*, Sousse, Tunisia, 2013, pp. 1–5, doi: 10.1109/ICCAT.2013.6521984.
[5] F. Boone and K. Wu, "Mode conversion and design consideration of integrated nonradiative dielectric (NRD) components and discontinuities," *IEEE Trans. Microw. Theory Techn.*, vol. 48, no. 4, pp. 482–492, Apr. 2000.
[6] B. Ghosh, N. R. S. Simons, L. Shafai, A. Ittipiboon, and A. Petosa, "TLM-based modal-extraction approach for the investigation of discontinuities in the rectangular waveguide and the NRD," *IEEE Trans. Microw. Theory Techn.*, vol. 50, no. 10, pp. 2294–2304, Oct. 2002.
[7] J. A. Monsoriu, B. Gimeno, E. Silvestre, and M. V. Andres, "Analysis of inhomogeneously dielectric filled cavities coupled to dielectric-loaded waveguides: Application to the study of NRD-guide components," *IEEE Trans. Microw. Theory Techn.*, vol. 52, no. 7, pp. 1693–1701, Jul. 2004.
[8] Y. Tsuji and M. Koshiba, "Finite element method using port truncation by perfectly matched layer boundary conditions for optical waveguide discontinuity problems," *J. Lightw. Technol.*, vol. 20, no. 3, pp. 463–468, Mar. 2002.
[9] J.-M. Jin, *The Finite Element Method in Electromagnetics*, 3rd ed. New York, NY, USA: Wiley, 2014.
[10] A. Taflove and S. C. Hagness, *Computational Electrodynamics-the Finite-Difference Time-Domain Method*, 3rd ed. Boston, MA, USA: Artech House, 2005.
[11] Y. Tsuji, K. Morimoto, A. Iguchi, T. Kashiwa, and S. Nishiwaki, "Two-dimensional full-vectorial finite element analysis of NRD guide devices," *IEEE Microw. Wireless Compon. Lett.*, vol. 31, no. 4, pp. 345–348, Apr. 2021.
[12] T. Bashir, K. Morimoto, A. Iguchi, Y. Tsuji, and T. Kashiwa, "Analysis of NRD guide devices using rigorous two-dimensional full-vectorial FDTD method," *Microw. Opt. Technol. Lett.*, vol. 65, no. 2, pp. 447–453, Feb. 2023.
[13] D. Li, P. Yang, and K. Wu, "An order-reduced volume-integral equation approach for analysis of NRD-guide and H-guide millimeter-wave circuits," *IEEE Trans. Microw. Theory Techn.*, vol. 53, no. 3, pp. 799–812, Mar. 2005.
[14] M. Bozzi, D. Li, S. Germani, L. Perregrini, and K. Wu, "Analysis of NRD components via the order-reduced volume-integral-equation method combined with the tracking of the matrix eigenvalues," *IEEE Trans. Microw. Theory Techn.*, vol. 54, no. 1, pp. 339–347, Jan. 2006.
[15] X. Lu, Z. Cao, M. C. van Beurden, Y. Jiao, Q. Wu, and T. Koonen, "A mode-matching method for three-dimensional waveguides with PMLs combined with energy conservation," *J. Lightw. Technol.*, vol. 36, no. 23, pp. 5573–5579, Sep. 11, 2018.
[16] R. C. Rumpf, "Improved formulation of scattering matrices for semi-analytical methods that is consistent with convention," *Prog. Electromagn. Res. B*, vol. 35, pp. 241–261, 2011.
[17] J. Liu, C. F. Tong, W. Jiang, and Q. H. Liu, "3-D NMM method for fully anisotropic and nonreciprocal media," *IEEE Trans. Microw. Theory Techn.*, vol. 70, no. 7, pp. 3428–3441, Jul. 2022.
[18] P. Lin Ho and Y. Yan Lu, "A stable bidirectional propagation method based on scattering operators," *IEEE Photon. Technol. Lett.*, vol. 13, no. 12, pp. 1316–1318, Dec. 2001.
[19] S. Wu and J. Xiao, "An efficient semivectorial bidirectional beam propagation method for 3-D optical waveguide structures," *J. Lightw. Technol.*, vol. 34, no. 4, pp. 1313–1321, Dec. 23, 2016.
[20] A. M. A. Said, A. M. Heikal, N. F. F. Areed, and S. S. A. Obayya, "Why do field-based methods fail to model plasmonics?" *IEEE Photon. J.*, vol. 8, no. 5, pp. 1–13, Oct. 2016.
[21] A. Iguchi, K. Morimoto, and Y. Tsuji, "Bidirectional beam propagation method based on axi-symmetric full-vectorial finite element method," *IEEE Photon. Technol. Lett.*, vol. 33, no. 14, pp. 707–710, Jul. 14, 2021.
[22] P. I. Davies and N. J. Higham, "A Schur–Parlett algorithm for computing matrix functions," *SIAM J. Matrix Anal. Appl.*, vol. 25, no. 2, pp. 464–485, Jan. 2003.
[23] C. Moler and C. Van Loan, "Nineteen dubious ways to compute the exponential of a matrix, twenty-five years later," *SIAM Rev.*, vol. 45, no. 1, pp. 3–49, Jan. 2003.
[24] J. Corones and R. Krueger, "Obtaining scattering kernels using invariant imbedding," *J. Math. Anal. Appl.*, vol. 95, no. 2, pp. 393–415, Sep. 1983.

HYUNUK AHN (Student Member, IEEE) received the B.S. degree in electronic engineering from the Muroran Institute of Technology, Muroran, Japan, in 2023, where he is currently pursuing the master's degree.

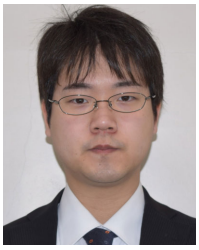

AKITO IGUCHI (Member, IEEE) received the B.S., M.S., and Ph.D. degrees in electronic engineering from the Muroran Institute of Technology, Muroran, Japan, in 2015, 2017, and 2019, respectively. From 2019 to 2020, he was a Postdoctoral Research Fellow of the Japan Society for the Promotion of Science (JSPS). He is currently an Assistant Professor with the Muroran Institute of Technology. He is a member of the Institute of Electronics, Information and Communication Engineers (IEICE), and Optica.

KEITA MORIMOTO (Member, IEEE) received the B.S., M.S., and Ph.D. degrees in electronic engineering from the Muroran Institute of Technology, Muroran, Japan, in 2017, 2019, and 2021, respectively. From 2021 to 2022, he was a Postdoctoral Research Fellow of the Japan Society for the Promotion of Science (JSPS). He is currently an Assistant Professor with the University of Hyogo. He is a member of the Institute of Electronics, Information and Communication Engineers (IEICE).

YASUHIDE TSUJI (Senior Member, IEEE) received the B.S., M.S., and Ph.D. degrees in electronic engineering from Hokkaido University, Sapporo, Japan, in 1991, 1993, and 1996, respectively. In 1996, he joined the Department of Applied Electronic Engineering, Hokkaido Institute of Technology, Sapporo, Japan. From 1997 to 2004, he was an Associate Professor of electronics and information engineering with Hokkaido University. From 2004 to 2011, he was an Associate Professor of electrical and electronic engineering with the Kitami Institute of Technology, Kitami, Japan. Since 2011, he has been a Professor of information and electronic engineering with the Muroran Institute of Technology, Muroran, Japan. His current research interest includes wave electronics. He is a member of the Japan Society of Applied Physics. He is a Senior Member of the Institute of Electronics, Information and Communication Engineers (IEICE), and Optica. In 1997, 1999, and 2019, he was awarded the Best Paper Award from IEICE. In 2000, he was a recipient of the Third Millennium Medal from IEEE. In 2019, he was a recipient of the IEEE Photonics Technology Letters Outstanding Reviewer Award. In 2021, he was a recipient of the Electronics Society Award from IEICE.